Computers & Geosciences 53 (2013) 129–140

Contents lists available at SciVerse ScienceDirect

Computers & Geosciences

journal homepage: www.elsevier.com/locate/cageo

CarboCAT: A cellular automata model of heterogeneous carbonate strata

Peter M. Burgess *

Department of Earth Sciences, Royal Holloway University of London, Egham, Surrey, TW20 0EX, UK

ARTICLE INFO

Article history:
Received 9 March 2011
Received in revised form
4 August 2011
Accepted 27 August 2011
Available online 21 September 2011

Keywords:
Carbonates
Stratigraphic forward modeling

ABSTRACT

CarboCAT is a new numerical model of carbonate deposystems that uses a cellular automata to calculate lithofacies spatial distributions and hence to calculate the accumulation of heterogeneous carbonate strata in three dimensions. CarboCAT includes various geological processes, including tectonic subsidence, eustatic sea-level oscillations, water depth-dependent carbonate production rates in multiple carbonate factories, lateral migration of carbonate lithofacies bodies, and a simple representation of sediment transport. Results from the model show stratigraphically interesting phenomena such as heterogeneous strata with complex stacking patterns, laterally discontinuous subaerial exposure surfaces, nonexponential lithofacies thickness distributions, and sensitive dependence on initial conditions whereby small changes in the model initial conditions have a large effect on the final model outcome. More work is required to fully assess CarboCAT, but these initial results suggest that a cellular automata approach to modeling carbonate strata is likely to be a useful tool for investigating the nature and origins of heterogeneity in carbonate strata.

1. Introduction

Many numerical stratigraphic forward models have successfully replicated large-scale aspects of carbonate stratal architectures (e.g., Bosence and Waltham, 1990; Aurell et al., 1998; Paterson et al., 2006; Williams et al., 2011). These models have helped to explain how various features of carbonate strata were produced. Fewer models have successfully reproduced the finer scale heterogeneity observed in carbonate strata, the origins of which remain relatively mysterious. Notable examples of finer-scale models include Parcell (2003) and Hasler et al. (2008) modeling fine-scale aspects of reef and platform interior lithologies from the Jurassic and Devonian, respectively, both using a partly stochastic approach. Burgess and Wright (2003) also used a partly stochastic approach to model cyclical platform interior strata that could develop as a consequence of island and shoreline migration, though heterogeneity was represented as a distribution of sub-, inter-, and supratidal strata without assigning specific lithologies to each water depth class. This work has made limited progress towards understanding the origins of carbonate platform margin and platform interior heterogeneity, but use of stochastic methods is a limiting factor because such approaches assign at least some of the processes responsible for the strata to the vagaries of a pseudo random number generator, and in doing so reveals little about how the depositional processes might actually work.

Cellular automata are a type of discrete numerical model that may offer an at least partial solution to this problem because they can be entirely deterministic in their calculation, generate relatively complicated results from relatively simple rule-based computational algorithms, and are at least loosely related to biological concepts of space, competition, and population dynamics (Flake, 2000). Cellular automata are composed of a regular grid of cells, each of which has one of a finite, usually small, number of possible states (e.g., Wolfram, 2001). Cell state is determined with reference to surrounding cells some specified distance away, for example, one or two cells distant (Fig. 1). Other cells within this surrounding area are referred to as the current cell's neighborhood. Application of simple rules, for example, based on the number of cells in the neighborhood with the same state, is used to determine the future state of a cell at the next iteration, or generation, of a cell.

Drummond and Dugan (1999) used cellular automata to model the origins of rare lithofacies in carbonate strata, but with an important stochastic element, thus negating many of the advantages of a cellular automata approach described above. Burgess and Emery (2004) combined elements of the model used in Burgess and Wright (2003) with deterministic cellular automata to create heterogeneity and sensitive dependence in a modeled platform interior system. Results from Burgess and Emery (2004) illustrate the potential of cellular automata models for generating simulated heterogeneous platform top strata and hence better understanding the origins of such heterogeneity.

This paper describes a new cellular automata model called CarboCAT (CAT being short for Cellular AuTomata) that models multiple carbonate lithofacies deposited in a platform interior

* Tel.: +44 1784 414083.
E-mail address: p.burgess@es.rhul.ac.uk

0098-3004/$ - see front matter © 2011 Elsevier Ltd. All rights reserved.
doi:10.1016/j.cageo.2011.08.026

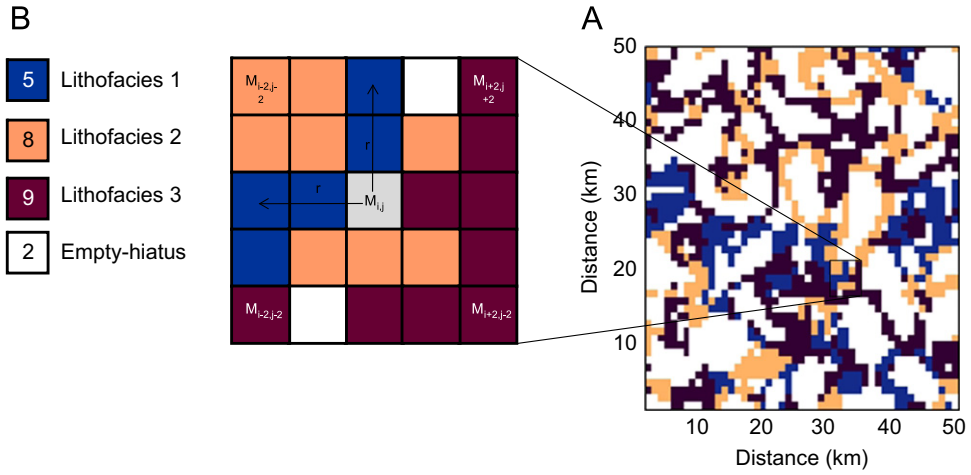

Fig. 1. An area of the model grid showing how the neighborhood of 24 cells around a central cell is defined. In the cellular automata model, persistence of a factory/lithofacies or occupation of empty cells by a particular factory depends on the count of same-factory cells within a 24-cell neighborhood.

setting is entirely deterministic, and yet can generate rich dynamic behavior and produce heterogeneous carbonate strata. CarboCAT is being developed as part of the CSDMS carbonate focused research group efforts to create a new generation forward model for carbonate platform strata.

2. Model formulation

2.1. Coding and runtime details

CarboCAT is written in Matlab 7.6.0 as a series of M files with a GUI front end that allows the user to specify an input parameter file and initialize and run the model. Model output is plotted in additional Matlab graphics windows.

2.2. The model grid

CarboCAT uses three-dimensional arrays to store calculated properties of model-led strata. These arrays have dimensions x, y, t, where x and y are planform map dimensions, and t is elapsed model time. Three of these arrays are defined, one for lithofacies, one for thickness, and one for depositional water depth. Since thickness is stored at each cell and each layer is coded by time, a geological cross section or a chronostratigraphic diagram can be easily constructed from the model output color coded according either to facies or to water depth of deposition.

Importantly, model cells have no intrinsic defined scale in the model. A particular scale is only implied by the parameters chosen for the model. For example, if high rates of sediment transport are specified, or if lithofacies lateral migration occurs at a particular rate, this has implications for cell size; 10 km by 10 km cells might be considered too big in this case, whereas 10 m by 10 m cells might be too small. Fixing a scale in the model based on more realistic representation of physical processes such as sediment transport remains an area for further work.

2.3. Carbonate production

CarboCAT uses a deterministic cellular automata to calculate what lithofacies is present in each cell on a 2D grid of 50 by 50 cells that represents a map view of an area of a carbonate platform top (Fig. 1A). Each cell in the model can be in one of four states, containing either one of the three types of carbonate factory shown in Fig. 2, or empty. The carbonate factory concept is

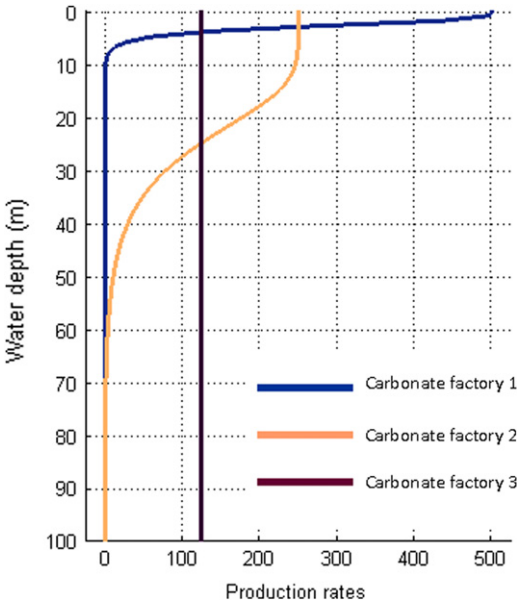

Fig. 2. Three production water-depth profiles used for the three carbonate factories in the CarboCAT models in this paper. Carbonate Factory One is a very shallow euphotic type, restricted to very shallow water production, representing organisms needing high light levels but producing carbonate material at a rapid rate. Factory Two is also euphotic but extends to greater water depths, representing organisms able to tolerate lower light levels than in Factory One, but producing at a lower maximum rate than Factory 1. The third factory produces carbonate material at a lower rate than Factories One and Two, but is aphotic, so produces at a rate independent of water depth (Fig. 2). It is assumed in these model runs that these are three different factories present in one location, for example, on a tropical carbonate platform top.

explained in Schlager (2005), Wright and Burgess (2005), and Pomar and Hallock (2008). In summary, different groups of carbonate producing organisms that make up a particular factory produce different types of carbonate material (e.g., rigid framework material, loose sand, mud etc.) at a characteristic range of water depths and under characteristic temperature and seawater chemistry conditions. In the model runs presented here three different factory types are defined, one restricted to very shallow water production, one extending to greater depths, and the third producing carbonate material at a lower rate but independent of water depth (Fig. 2). This configuration of factories is intended to demonstrate how CarboCAT can model strata that might result

from the close spatial juxtaposition of three different groups of tropical carbonate producing organisms. Many other configurations are possible, for example, several factories with the same depth-production profile but producing different lithologies.

For each iteration of the model, simple rules are applied to determine the state of each cell at the next iteration or time step. These rules are summarized in Table 1 and are based on definition of a neighborhood composed of the surrounding 24 cells (Fig. 1B). The rules are intended as an approximate representation of principles of spatial competition and resource availability, and resulting minimum and maximum thresholds of population size required for survival, but as such are rather poorly constrained due to sparse data on competition. A cell persists in its current state occupied by a particular factory when

$4 \le n \le 10$,

where n is the number of cells in the neighborhood with the same factory type. This rule represent a situation where environmental and competition conditions are favorable to continuation of the factory; the area is not overcrowded, but nor is it underpopulated and vulnerable. A cell becomes empty when

$n \le 3$ or $n \ge 11$.

This rule represents death of a factory whether due to overcrowding, or due to a decline in population to unsustainably small levels. Empty cells are colonised by a new factory when

$6 \le n \le 10$,

representing optimum living conditions offering the best chance for growth of new organisms. Note that the order of checking which factory type should occupy an empty cell is varied through time to avoid bias for a particular factory type. This is done by specifying the order of checking (e.g., 1,2,3; 2,3,1; 3,1,2) performed during each model time step. For each empty cell found during this time step, suitability for being colonised by a carbonate factory is checked in this order, and the order is then changed for the next time step. Changing of order like this is optional; if one wanted to represent a system with clear competitive advantage in colonization, this could be encoded in the order of checking empty cells, the most aggressive factory type (Fig. 3). Accumulation of carbonate strata occurs only in cells occupied by a carbonate factory, and accumulation rate is calculated using a water-depth production profile based on the euphotic curves from Bosscher and Schlager (1992). These curves were derived from data for the main Caribbean reef-building coral (*Montastrea annularis*). They assume that carbonate production is a hyperbolic tangent function of water depth, such that

$$g_{(w)} = g_m \tanh\left(\frac{I_0 e^{-kw}}{I_{(c)}}\right),$$

Table 1
Rules for carbonate cellular automata.

Carbonate type	Neighborhood radius (cells)	Minimum neighbors	Maximum neighbors	Minimum trigger	Maximum trigger	Trigger carbonate type
1	2	4	10	6	10	1
2	2	4	10	6	10	2
3	2	4	10	6	10	3

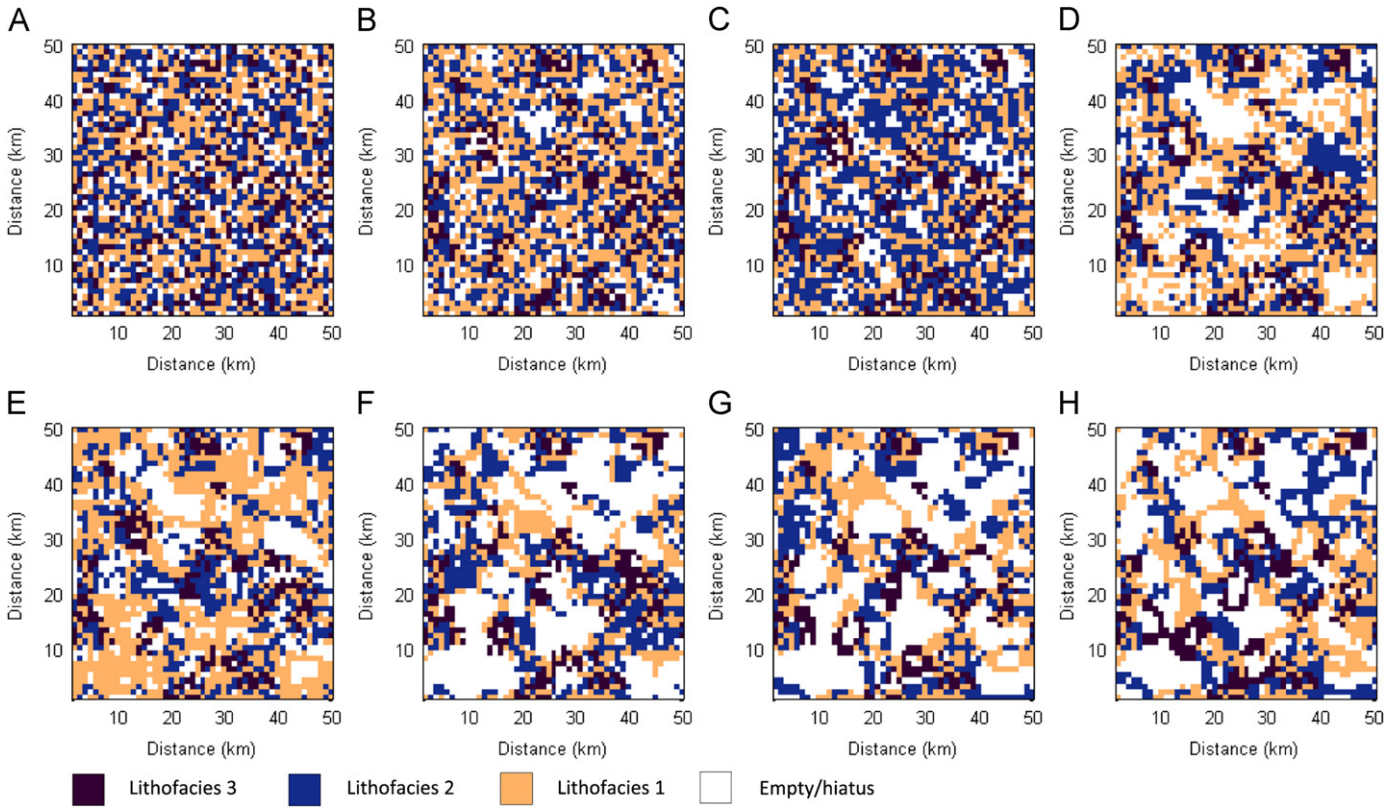

Fig. 3. Eight iterations of the model starting from a random initial condition at time step 0 (A) Note how successive iterations of the model, from iteration 1 in B to iteration 7 in H show how operation of the cellular automata decreases spatial entropy (see Fig. 5) by increasing clustering of the lithofacies and adding structure to the spatial distribution of lithofacies.

where w is water depth in meters, $g_{(m)}$ is a maximum rate of growth in m My^{-1}, I_0 is surface light intensity, I is saturation light intensity, and c is extinction coefficient. This can be expressed in terms of carbonate accumulation rate, e, instead of growth rate and applied in the model as

$$e_{(w)} = e_m \tanh(k\exp(dw_{(t)})),$$

where w is water depth in m, d is a decay constant, m is maximum production rate in m My^{-1}, and k is a rate constant. Each factory can have a different production profile and maximum production rate (see Fig. 2 and Table 2 for examples of rates used in these model runs). To represent the influence of competition on production rate, maximum production rate for a particular cell at a particular time varies due to the number of same-factory neighbors in the surrounding 24 cells, so

$$n < n_{\min} : a = 0$$

$$4 \le n < n_{\text{optimum}} : \; a = e_w \frac{n-(n_{\min}-1)}{n_{\text{optimum}}-(n_{\min}-1)}$$

$$N = n_{\text{optimum}} : a = e_{(w)}$$

$$n_{\text{optimum}} < n < n_{\max} : a = e_w \frac{(n_{\max}+1)-n}{(n_{\max}+1)-n_{optimum}}$$

$$n > = n_{\max} : a = 0$$

where n is the number of same-factory neighbors for any given cell, $n_{\min}$ and $n_{\max}$ are the minimum and maximum neighbors, respectively required for a cell to survive into the next generation, and n_{optimum} is the number of neighbors required for maximum production rate. These equations represent a simple linear increase from minimum production with the minimum number of neighbors to maximum production at the optimum number of neighbors, and a linear decrease to minimum production rate with the maximum number of neighbors. Hence, production rate varies according to water depth but also spatially across the model grid according to the evolving location, size, and shape of the carbonate factory areas.

Lithofacies deposition is modeled by assuming that each factory produces and accumulates a different lithofacies, so for these model runs model strata consist of three lithofacies. Empty cells are considered to represent a depositional hiatus during which accumulation rate is zero and can be colonised by one of three factory types, at which point the cell will begin to accumulate strata of the lithology type produced by that factory.

2.4. Carbonate sediment transport

Although much deposition on carbonate platform tops occurs due to in situ production of carbonate material, sediment transport clearly occurs and plays an important role in accumulation, and in development of spatial and therefore vertical facies distributions and heterogeneity. In order to include a very simple representation of sediment transport in CarboCAT without requiring significantly more computational power and more information on other physical parameters such as currents, sediment transport is modeled using a very simple gradient-based method to distribute a proportion of produced sediment into adjacent lower elevation model cells not already occupied by producing carbonate facies. The algorithm is explained with a hypothetical example in Fig. 4. Thickness of sediment to be transported from any grid cell is calculated via a user-specified proportion of the total thickness of sediment produced, and the lithofacies of the transported sediment is also specified, allowing an in situ production lithofacies to generate a different lithofacies of transported sediment.

Sediment to be transported from the original producing cell is divided equally among any adjacent lower elevation cells. If these cells have adjacent lower cells too, half of the sediment transported to the cell is deposited, and the remaining half is split between the adjacent lower cells. Otherwise, if none of the adjacent cells are lower elevation, all the sediment transported to the cell is deposited in the cell. Once sediment thickness being

Table 2
Model parameters for the four model runs described in the paper.

Model parameter	Model run No.			
	1	2	3	4
Total iterations	1000	1000	1000	1000
Time step (My)	0.01	0.01	0.01	0.01
Initial water depth (m)	2	2	2	2
Subsidence rate (m My^{-1})	50	50	50	50
Eustasy period 1 (My)	na	0.50	na	na
Eustasy amplitude 1 (m)	na	20	na	na
Eustasy period 2 (My)	na	0.15	na	na
Eustasy amplitude 2 (m)	na	5	na	na
Lithology 1 carbonate production rate (m My^{-1})	500	500	500	500
Lithology 1 Surface light intensity (μE m^{-2} s^{-1})	2000	2000	2000	2000
Lithology 1 extinction coefficient	0.8	0.8	0.8	0.8
Lithology 1 saturating light (μE m^{-2} s^{-1})	300	300	300	300
Lithology 1 transport product facies	na	na	4	na
Lithology 1 transported fraction of total production	na	na	0.75	na
Lithology 2 carbonate production rate (m My^{-1})	400	400	400	400
Lithology 2 Surface light intensity (μE m^{-2} s^{-1})	2000	2000	2000	2000
Lithology 2 extinction coefficient	0.1	0.1	0.1	0.1
Lithology 2 saturating light (μE m^{-2} s^{-1})	300	300	300	300
Lithology 2 transport product facies	na	na	5	na
Lithology 2 transported fraction of total production	na	na	0.25	na
Lithology 3 carbonate production rate (m My^{-1})	100	100	100	100
Lithology 3 Surface light intensity (μE m^{-2} s^{-1})	2000	2000	2000	2000
Lithology 3 extinction coefficient	0.005	0.005	0.005	0.005
Lithology 3 saturating light (μE m^{-2} s^{-1})	300	300	300	300
Lithology 2 transport product facies	na	na	na	na
Lithology 3 transported fraction of total production	na	na	na	na

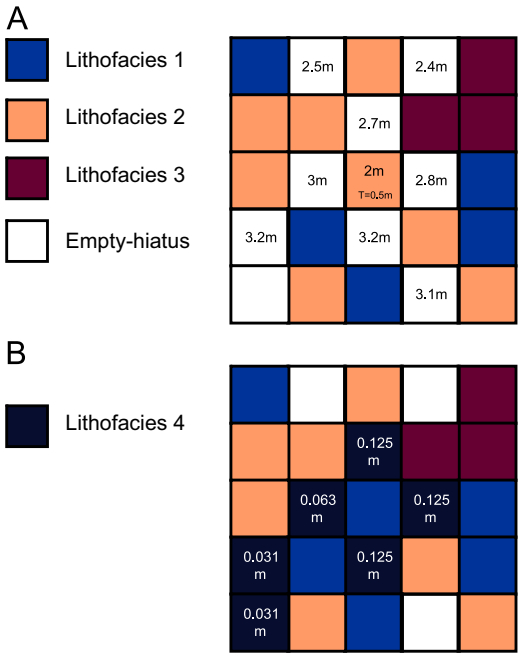

Fig. 4. Sediment transport is calculated at each iteration from each cell on the grid occupied by a producing carbonate factory. A proportion of produced sediment, in this example 0.5 m, is transported from the source cell to adjacent lower elevation shown in A. Transport continues to any adjacent lower elevation cells, or until insufficient thickness of sediment remains to transport. (B) Shows the final outcome of transport from the central cell for this configuration of facies and elevations.

transported in a cell drops below a threshold of 0.5 cm transport stops and the remaining sediment is deposited. The consequence of this algorithm is that sediment will be transported a characteristic distance from a source cell, depending on the fraction deposited at each step, and depending on the bathymetry of the current model surface which may or may not provide a suitable route for the transported sediment to run out down slope. For any particular bathymetry, a greater thickness of transported sediment, and a smaller proportion deposited at each step en route, will lead to a longer transport distance.

Note that the transport parameter values described above are entirely arbitrary and can be easily modified; further sensitivity analysis and, most importantly, comparison between modeled CarboCAT strata and outcrop of modern systems is required. A more "transport-dominated" system would have a higher proportion of produced sediment being initially transported than would a system producing framework carbonate more resistant to breakdown and transport, and might also have a smaller proportion of the transported sediment being deposited at each point along the transport route.

2.5. Relative sea level

Subsidence is modeled very simply using a single spatially and temporally invariant rate for the whole model grid. Eustatic oscillations are calculated using simple sinusoids with up to three different periods and amplitudes. When relative sea-level fall results in subaerial exposure of a cell, accumulation stops and any carbonate factory in that cell becomes dormant. When the cell refloods the cell reactivates with the same factory and accumulation may resume. However, any seafloor bathymetry may mean that cells reflood before surrounding cells and have too few neighbors to survive, in which case a relative sea-level fall and rise that exposes and refloods the platform may reset the spatial distribution of the carbonate factories quite significantly, as would be expected to happen on a real platform top.

2.6. Recording carbonate accumulation

Strata accumulate in the real world as a consequence of subsidence, carbonate production in different factories, sediment breakdown and transport, and relative sea-level oscillations, plus probably many other processes, that act through geological time to create layers of carbonate rock of variable lithology. CarboCAT follows the same basic process; layers of modeled strata are generated as a consequence of subsidence creating accommodation, carbonate production generating a spatial distribution of in this case three lithofacies, sediment transport breaking down and

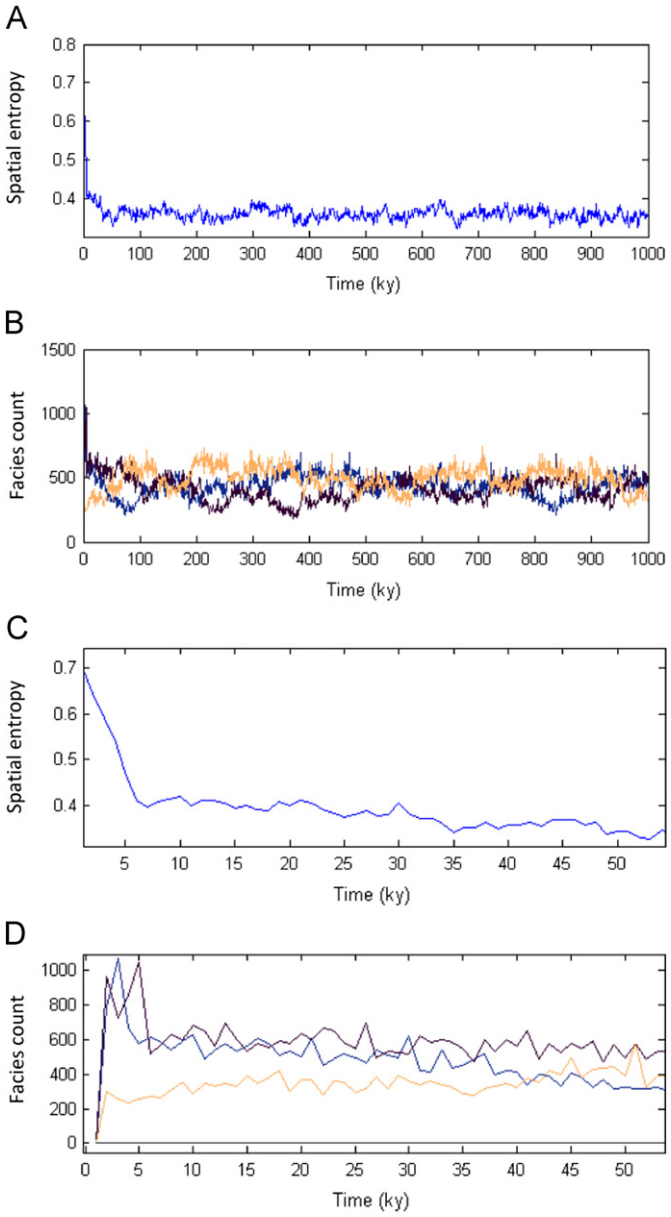

Fig. 5. (A) Spatial entropy and (B) lithofacies counts for each of the 1000 iterations in Model Run 1. Note how facies numbers vary dynamically but entirely deterministically around a value of approximately 500, one-fifth of the total 2500 cells on the model grid. (C) Spatial entropy and (D) lithofacies counts for the first 50 iterations in Model Run 1 showing how spatial entropy rapidly decreases from the initial high of the random initial condition (see Fig. 4) and facies numbers approach a dynamic equilibrium around 500.

redepositing material as two new lithofacies, and relative sea-level oscillations creating and destroying accommodation.

To achieve this, the model operates as a series of time steps, calculated forward in time from a user-specified initial condition (Fig. 3A). A layer of strata is then calculated for each subsequent time step based on the distribution of lithofacies calculated for each time step (Fig. 3B–H) that produce sediment at different rates. Accumulated thickness in each grid cell for the current time step is a product of either sediment production or sediment transport, or some combination of both.

For each model time step, the following occurs:

1. Water depth is updated from the bathymetry calculated in the previous time step, adding accommodation, based on the specified subsidence rate.
2. Elevation of sea level is calculated from the specified eustatic sea-level curve and the water depth across the grid is updated accordingly.
3. A new factory/facies mosaic is calculated based on the state from the previous time step following the cellular automata rules described above (e.g., the previous time step is time step 4 (Fig. 3E), and the new time step factory mosaic is time step 5 (Fig. 3F)).
4. Thickness of carbonate strata produced for the time step is calculated as a function of water depth and the production rate–depth curve for the factory present in each cell.
5. Sediment transport is then calculated from each cell, with thickness added to appropriate surrounding cells as described above.

This process is repeated for the specified number of time steps, and the strata are recorded in the model grid three-dimensional arrays described above. Contents of these arrays can then be analyzed and plotted at the end of the model run to generate the output seen in Fig. 3 and Figs. 5–11.

2.7. *Spatial entropy, aggradation progradation ratios, and the KS test*

Spatial entropy is another useful metric for quantifying heterogeneity, particularly in models like this that show an

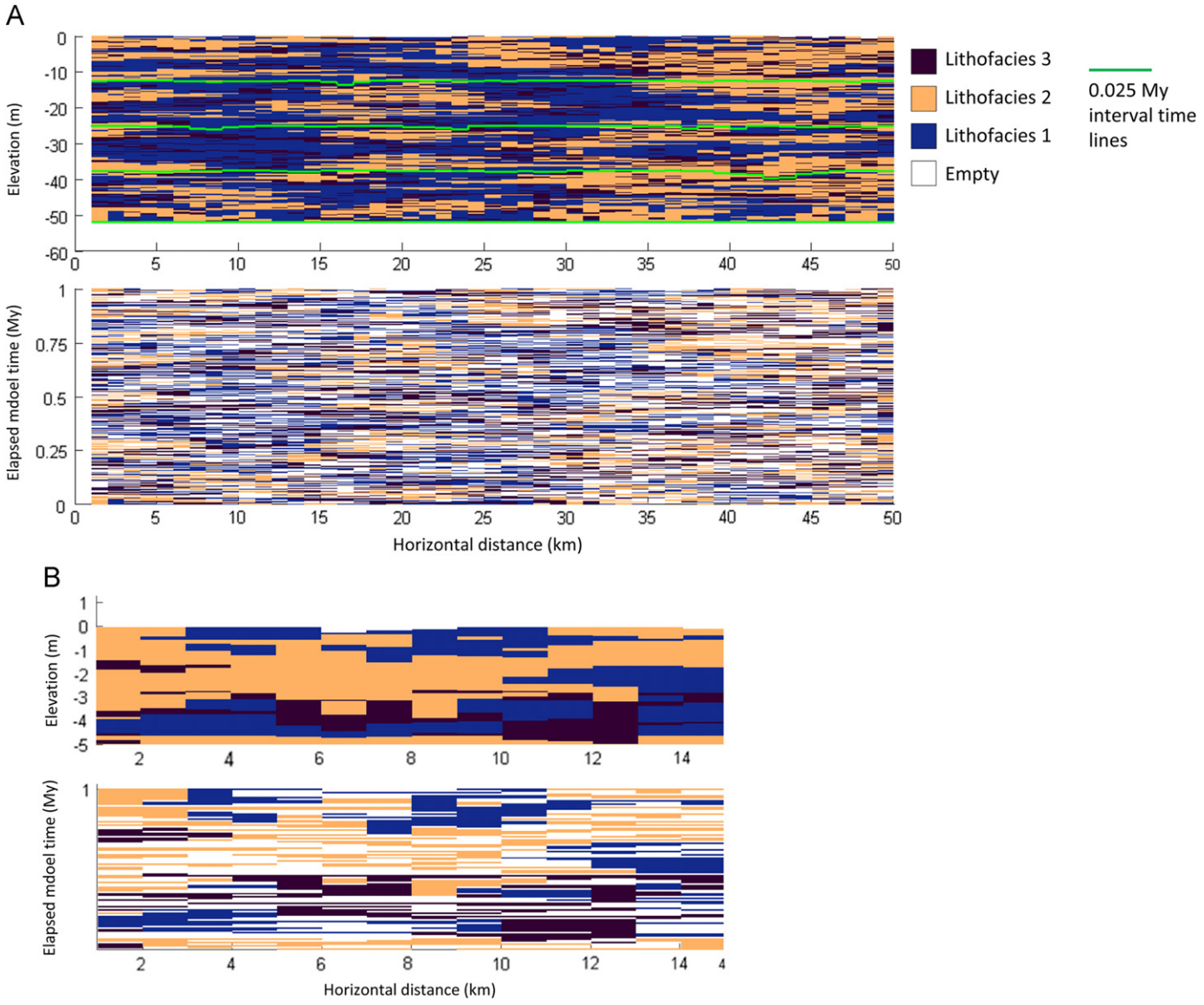

Fig. 6. (A) Cross section and chronostratigraphic diagram from $x=25$ showing strata deposited over 1 h My. Lateral and vertical heterogeneity is apparent in both depth and geological time sections. Hiatuses are present throughout the strata visible in the chronostratigraphic diagram. (B) A zoomed view from the top left of A) showing the depth and time view of the stratal bodies developed in the model.

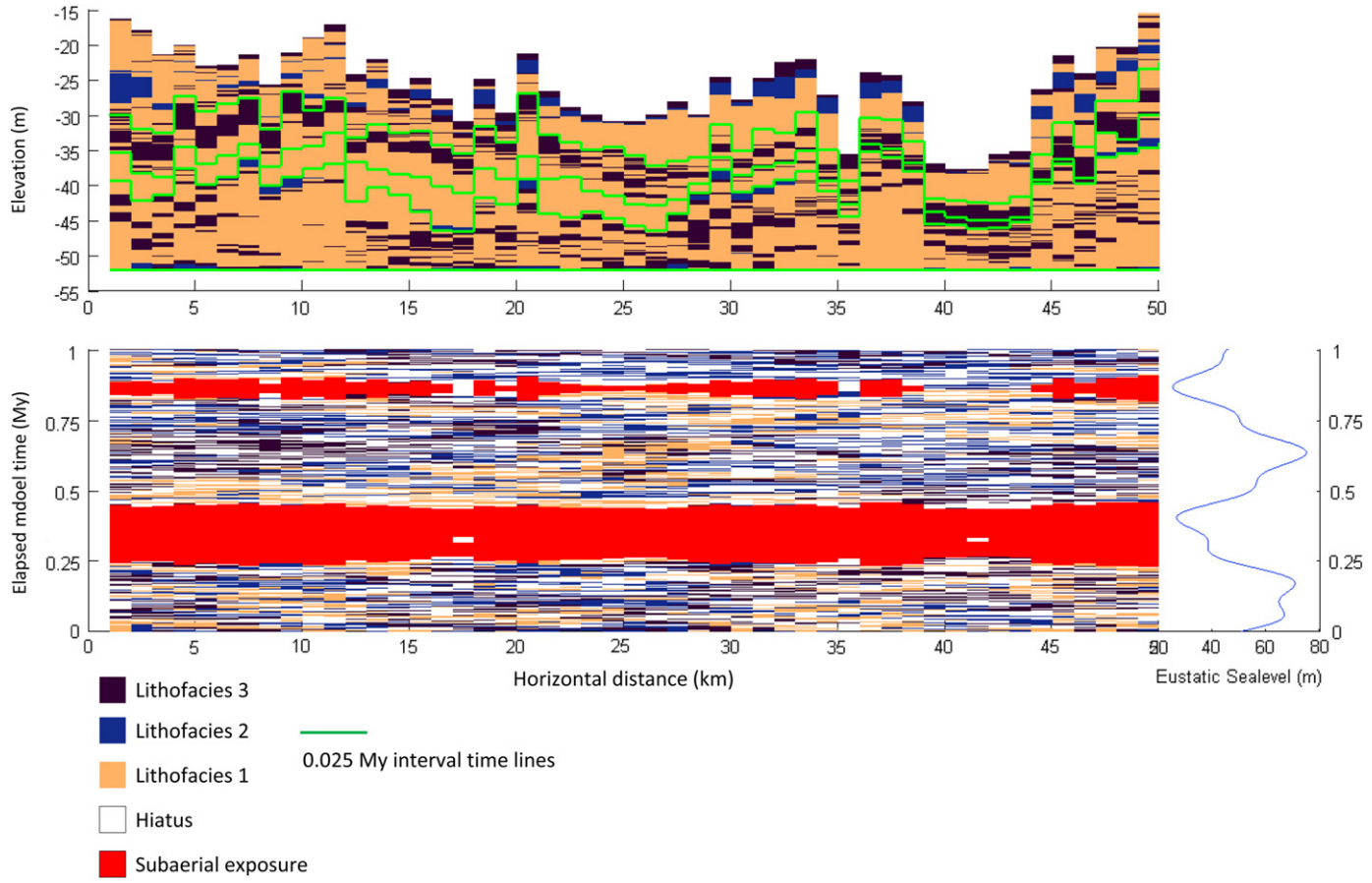

Fig. 7. A depth cross section and a chronostratigraphic diagram from $x=25$ showing strata deposited in Model Run 2 with eustatic oscillations, also shown. Notable features are the up to 35 m of water depth developed by the end of the model run due to rate of accommodation creation outstripping rate of accumulation, and the variable lateral extent of the subaerial hiatus developed during the relative sea-level falls.

element of self-organization. Spatial entropy is calculated here following the method described in Drummond and Dugan (1999). Results from the calculation are shown in Fig. 5 and are discussed below in the results section below.

Stratal geometry is summarized in the model by the ratio of progradation to aggradation. This is calculated by counting the number of same-facies vertical transitions as aggradational and dividing by the number of vertical transitions to different facies that represent progradation. A vertical transition to a different facies represents progradation in this context because in order for the transition to a different facies to occur, lateral migration of a facies body must have occurred (e.g., see Fig. 6B). Since there is no proximal or distal reference on these particular model grids, the term progradation is here considered synonomous with lateral migration. The ratio of progradation to aggradation is of particular interest here because as well as capturing an essential element of stratal architecture, it presumably relates to the type of lithofacies thickness produced by the model.

Lithofacies thickness distributions generated by CarboCAT are compared to a theoretical exponential $F(t)$ calculated using the same mean lithofacies unit thickness following the method described in Burgess (2008) and Press et al. (1992), so

$$F(t)=1-e^{-\mu t},$$

where t is lithofacies thickness and μ is the mean lithofacies unit thickness. Modeled and theoretical curves are plotted on the same normalized axis, and the maximum offset or difference D between the two distributions can then be calculated. This value D forms the basis for the Kolmogorov–Smirnov test of the null hypothesis that the distribution being investigated is indistinguishable from an exponential distribution. The significance probability p of an observed value of difference D is calculated via

$$p=Q_{ks}(\lambda),$$

where

$$Q_{ks}(\lambda)=2\sum_{j=1}^{\infty}(-1)^{j-1}e^{-2j^2\lambda^2},$$

and the function parameter λ is given by

$$\lambda=(\sqrt{N}+0.12+0.11/\sqrt{N})D,$$

where N is the total number of lithofacies units in the modeled section. p is the probability that values of D at least as extreme as that observed could occur by chance sample variation if the distribution was indeed an exponential. Hence values of p close to zero indicate that the observed distribution is highly unlikely to be exponential, equivalent to rejecting the null hypothesis at a greater than 99% significance level. Values of p greater than or equal to 0.10 provide insufficient evidence to reasonably reject an exponential interpretation. In these cases an exponential distribution can be considered a good model to represent the observed thickness data.

2.8. Model output

2.8.1. Model run 1: constant sea-level run

Model Run 1 has 1000 iterations with a time step of 1 ky giving a total elapsed model time of 1 My, constant eustatic sea level,

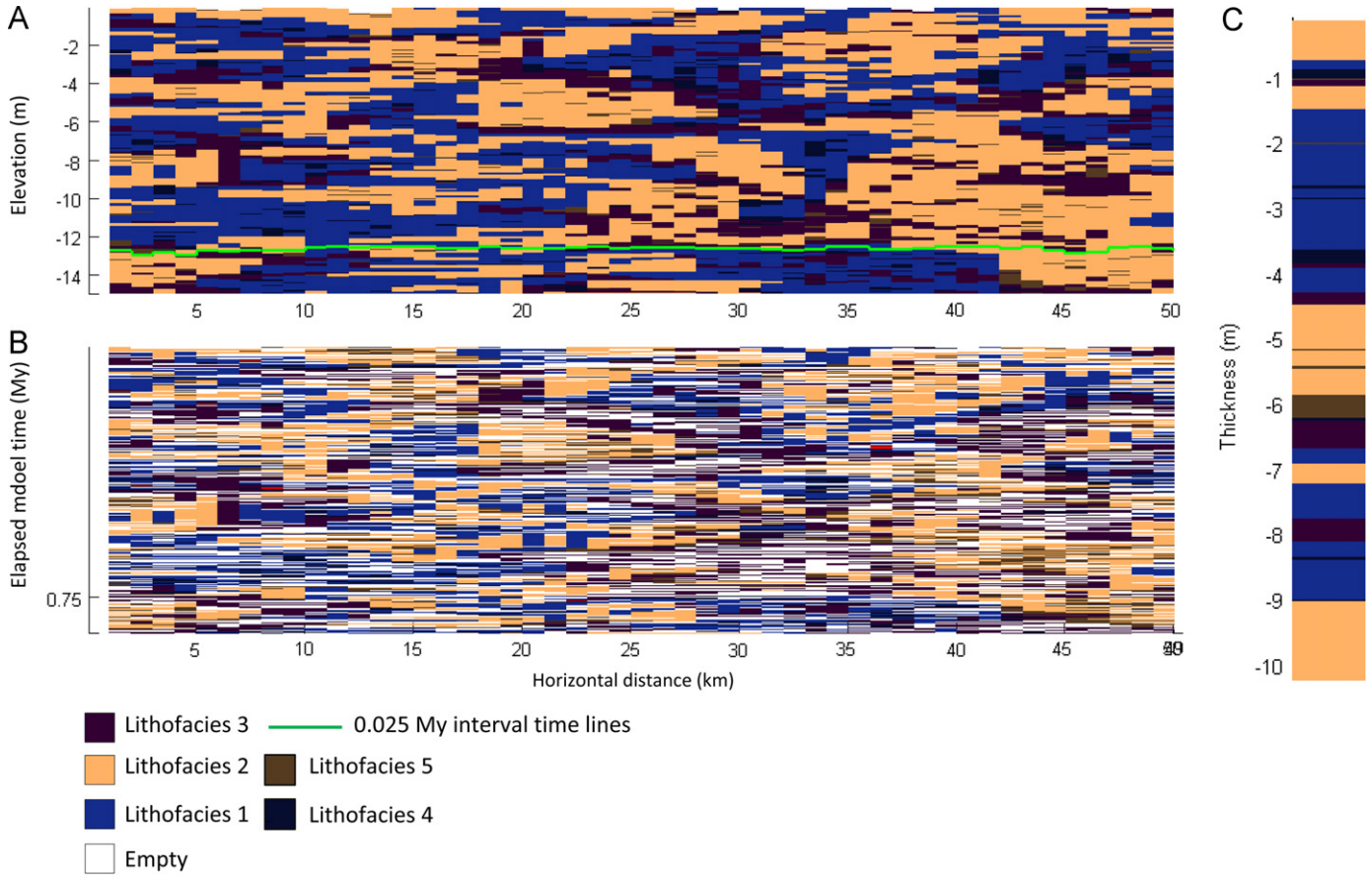

Fig. 8. A depth cross section (A) and a chronostratigraphic diagram (B), both from $x=25$ and a vertical section (C) all showing strata deposited in Model Run 3 which includes sediment transport. Lithofacies 4 and 5 are transported sediment and are visible in both the cross section, chronostratigraphic diagram, and the vertical section. Generally, the presence of additional transported lithofacies tends to increase heterogeneity.

rising relative sea level due to a subsidence rate of 50 m My^{-1}, and the other model parameters listed in Table 2. The model starts with a random spatial distribution of lithofacies, where each grid cell has an equal probability of being empty, or containing lithofacies 1–3 (Fig. 3A). These lithofacies represent products of three different carbonate factories operating in proximity to each other but populated by organisms with different light requirements (Fig. 2) as discussed above. Operation of the cellular automata over subsequent time steps acts to form clusters of each lithofacies (Fig. 3B–H) and reduce the spatial entropy from an initial value of ~0.7 to a time averaged value of 0.36 (Fig. 5). This is an example of self-organization whereby patterns emerge due to the internal dynamics of the system, without explicit external forcing (Drummond and Dugan, 1999; Wolfram, 2001). The resulting lithofacies planforms require further analysis and quantitative comparison with lithofacies maps from modern carbonate environments, but bear at least superficial resemblance to aspects of lithofacies planform patterns observed, for example, in Florida Bay (Wanless and Tagett, 1989). During the 1 My of elapsed model time the proportion of each lithofacies present varies in a dynamic equilibrium with the other lithofacies as they "compete" for space on the model grid (Fig. 5).

Strata accumulated during this model run are shown in Fig. 6A as a cross section with elevation on the vertical plot axis, and as a chronostratigraphic diagram with elapsed model time on the vertical axis. A more detailed view of a subset of the sections in Fig. 6A is shown in Fig. 6B. Both the chronostratigraphic diagram and the cross section demonstrate how carbonate strata generated by the model show a mixture of aggradational and progradational stacking and interfingering of the three lithofacies to create complex three-dimensional geobody geometries (see, for example, Larue and Hovadik (2006) for an explanation of the geobody concept). Different production rates for the three different lithofacies are reflected in the variable thicknesses of the three lithofacies and the resulting difference in lateral versus vertical extent of lithofacies geobodies (Fig. 6A and B) measured in the model as the progradation/aggradation ratio of 0.20 (see Table 3).

In this model run carbonate accumulation occurs in keep-up mode, filling accommodation to sea level. However, intermittent accumulation on the cellular automaton leads to increases in water depth (see top of the depth section in Fig. 6). One consequence of this is that time lines in the strata are not flat but rather show relief of up to a few meters even in this keep-up case. More generally, breaks in accumulation due to migration of carbonate producing areas on the cellular automata and turning on and off of production in individual cells lead to strata with a typical stratigraphic completeness value of 0.55 (see the chronostratigraphic diagram in Fig. 6B). Low stratigraphic completeness due to intermittent deposition seems a reasonable representation of carbonate deposition based on modern depositional surfaces with large areas of no accumulation (e.g., hardground mapped in the Arabian Gulf (Purkis et al., 2005)).

2.8.2. *Model run 2: variable sea-level run*

The second model run included two periods of eustatic oscillation with periods and amplitudes assumed typical for

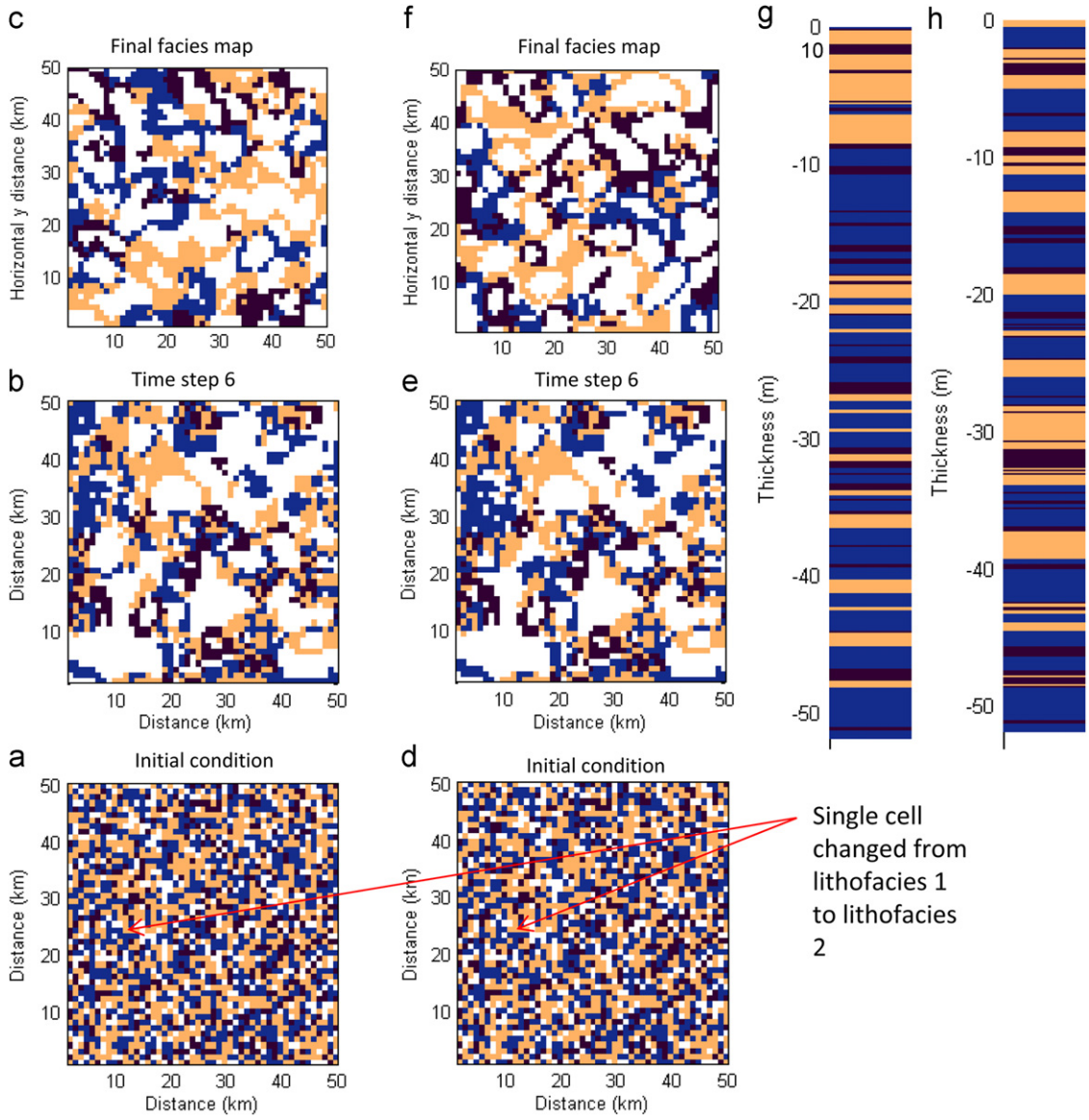

Fig. 9. Output from Model Run 1 and Model Run 4 which have identical parameters except for a different facies in a single cell in the initial facies map (a and d). Maps from subsequent iterations in the two model runs (b, c, e, and f) show how the spatial facies distributions diverge through time and lead to quite different vertical successions at $x=25$ $y=25$ (g and h).

greenhouse climatic settings (Table 2). During rising eustatic sea level, rate of accommodation creation outpaces accumulation rate and keep-up style accumulation is replaced by catch-up style accumulation. Spatially variable sediment accumulation leads to variable water depth, with a maximum of ~35 m and a minimum of 15 m. Unfilled accommodation and the resulting topographic relief on the platform top resulting from differential accumulation leads to laterally variable development of exposure surfaces during minor eustatic falls that are too small to expose the relatively deep-water areas of the platform (Fig. 7). Because of unfilled accommodation and spatially variable accumulation subaerial exposure surfaces for smaller eustatic falls are laterally discontinuous.

2.8.3. *Model run 3: the effects of sediment transport*

Adding sediment transport and keeping eustatic sea-level constant at 0 m leads to the output from Model Run 3 shown in Fig. 8. Two additional transported lithofacies derived from carbonate factories one and two are visible in the cross section, chronostratigraphic diagram and vertical section in Fig. 8. The third carbonate factory is assumed in this model run not to produce transportable material. The two transported lithofacies make up ~10% of planform area but are generally thinner than the in situ produced lithofacies. The presence of the transported lithofacies changes the progradation/aggradation ratio to 0.57 compared to a value of 0.20 without transport (see Table 2), showing that transported material does have an impact on the overall stratal architecture.

2.8.4. *Model run 4: sensitive dependence on initial conditions*

Burgess and Emery (2004) documented sensitive dependence on initial conditions in a carbonate forward model that included a cellular automata component. CarboCAT shows similar behavior. Fig. 9 shows results from Model Run 4 which has identical parameters to Model Run 1 except for the initial facies in one single cell in the model grid where the initial facies was changed from lithofacies 1 to lithofacies 2 (Fig. 9a and d). Intuition might suggest that such a small change in the initial conditions would

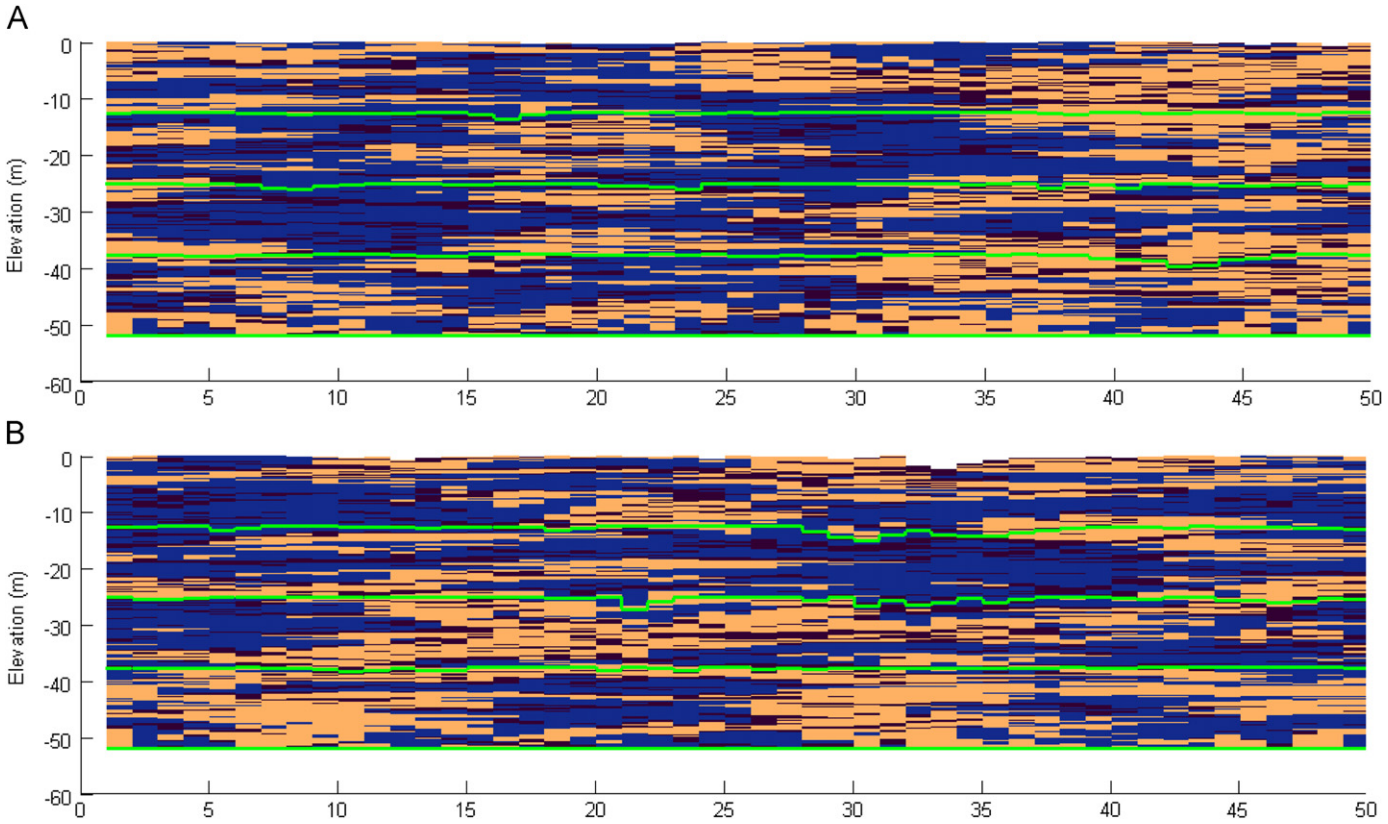

Fig. 10. Cross section from Model Run 1 (A) and Model Run 2 (B) which have identical parameters except for a different facies in a single cell on the initial facies map (see Fig. 9A and 9D). Note the quite different strata developed in each model, despite the very small difference in initial conditions.

have little or no effect, or that any effects of the different initial conditions would quickly dissipate, so that the final results of Model Run 4 and Model Run 1 would be similar. However, the opposite is true; the initial difference propagates across the model grid so that the final results in the two models differ greatly in the detailed spatial positions of particular facies (Figs. 9 and 10), though in terms of overall statistical properties like spatial entropy, they remain similar (Table 3). This is an example of sensitive dependence on initial conditions, and if this kind of behavior occurs in natural carbonate systems it has significant implications for understanding and reconstructing the details of a facies succession, as well as predicting carbonate strata away from data points. More work with CarboCAT is required to investigate this behavior in more detail.

2.9. Comparison of modeled lithofacies thickness distributions with a theoretical exponential

An important feature observed in carbonate strata is their lithofacies thickness distribution. Wilkinson and Drummond (2004) pointed out that such strata commonly exhibit a lithofacies thickness distribution with many more thin than thick units that can be usefully represented as exponential distributions. Burgess (2008) followed this up with an analysis that showed that around one third of an outcrop dataset are indeed exponential, while one third are ambiguous and one-third are likely not exponential. Based on this an important aspect of a model of fine-scale carbonate heterogeneity would seem to be the types of lithofacies thickness distribution it can produce and how these compare with outcrop examples.

Fig. 11 shows vertical sections, lithofacies distributions, and theoretical exponential distributions calculated for Model Runs 1, 2, and 3. In each case the modeled distribution is taken from the central point on the model grid, so $x=25$, $y=25$, and total thickness varies largely as a consequence of either a keep-up (Model Runs 1 and 3) or catch-up style of deposition (Model Run 2). In each case, results from the KS test give low P values that clearly indicate that the modeled lithofacies thickness distributions are not a good match with an exponential curve. All the examples show too few thin beds compared to the exponential, making them somewhat similar to Pennsylvanian outcrop examples included in the database in Burgess (2008). However, with only four model runs to consider, conclusions about the significance of the lack of fit to an exponential, and similarity to outcrop examples, are probably premature. More work is required to analyze the lithofacies thickness output generated by CarboCAT with a wider range of parameters, for example, using the approach implemented in Burgess and Pollitt (in press). Note, however, that this approach typically requires thousands of model runs and thus will likely require significant processing power to complete.

3. Conclusions

CarboCAT is a simple and entirely deterministic forward model of platform interior carbonate strata that, despite its simplicity and lack of stochastic elements, produces heterogeneous platform interior strata and exhibits stratigraphically interesting behaviors. These behaviors include complex histories of lateral migration and interfingering of lithologies, development of complex bathymetries related to lateral changes in carbonate accumulation rate, development of laterally variable and discontinuous subaerial exposure surfaces during relative sea-level fall, and sensitive dependence to initial conditions leading to quite different occurrences of lithofacies with only very small changes in the model initial conditions. These preliminary results suggest that more

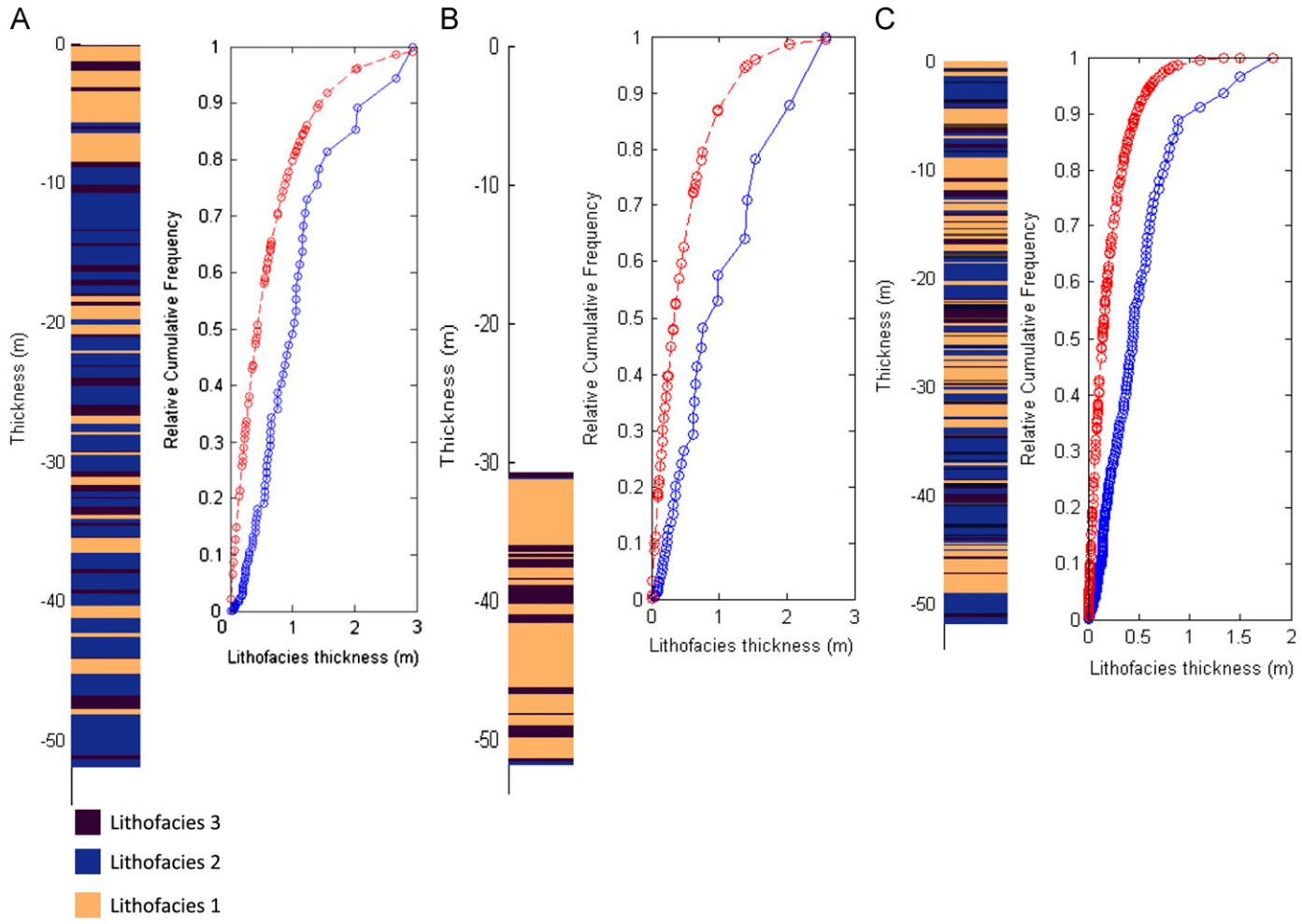

Fig. 11. Vertical sections, lithofacies thickness distributions from Model Runs 1, 2, and 3, and equivalent theoretical exponential distributions. KS test results show that for all three models the distributions are not exponential.

Table 3
Model run results.

Model run No.	Model description	P/A ratio	Spatial entropy	Stratigraphic completeness	*P* value	Curve type
1	No transport, constant eustasy	0.2026	0.36	0.55	0.000	Nonexponential
2	No transport, dual period eustasy	0.1004	0.29	0.42	0.000	Nonexponential
3	With transport, constant eustasy	0.5729	0.43	0.66	0.000	Nonexponential
4	No transport, constant eustasy	0.2029	0.36	0.55	0.000	Nonexponential

work is required to fully assess CarboCAT, and that a cellular automata approach to modeling carbonate strata is likely to be useful for investigating the nature and origins of heterogeneity in carbonate strata.

References

Aurell, M., Badenas, B., Bosence, D.W.J., Waltham, D.A., 1998. Carbonate production and offshore transport on a Late Jurassic carbonate ramp (Kimmeridgian, Iberian basin, NE Spain): Evidence from outcrops and computer modelling. In: Wright, V.P., Burchette, T.P. (Eds.), Carbonate Ramps, 149. , The Geological Society, Special Publication, pp. 137–161.

Bosence, D.W.J., Waltham, D.A., 1990. Computer modeling the internal architecture of carbonate platforms. Geology 18, 26–30.

Bosscher, H., Schlager, W., 1992. Computer simulation of reef growth. Sedimentology 39 (3), 503–512.

Burgess, P.M., 2008. The nature of shallow-water carbonate lithofacies thickness distributions. Geology 36, 235–238.

Burgess, P.M., Emery, D.J., 2004. Sensitive dependence, divergence and unpredictable behaviour in a stratigraphic forward model of a carbonate system. In: Curtis, A., Wood, R. (Eds.), Geological Prior Information, 239. , Geological Society of London, Special Publication, pp. 77–94.

Burgess, P.M., Pollitt, D.A., in press. The origins of shallow-water carbonate lithofacies thickness distributions: 1D forward modelling of relative sea-level control. Sedimentology.

Burgess, P.M., Wright, V.P., 2003. Numerical forward modelling of carbonate platform dynamics: An evaluation of complexity and completeness in carbonate strata. Journal of Sedimentary Research 73, 637–652.

Drummond, C.N., Dugan, P.J., 1999. Self organizing models of shallow water carbonate accumulation. Journal of Sedimentary Research 69, 939–946.

Flake, G.W., 2000. The Computational Beauty of Nature: Computer Explorations of Fractals. Chaos, Complex Systems, and Adaptation, The MIT Press 514.

Hasler, C.A., Adams, E.W., Wood, R.A., Dickson, J.A.D., 2008. Fine scale forward modelling of a Devonian patch reef, Canning Basin, Western Australia. in: de Boer, et al. (Eds.), Analogue and Numerical Modelling of Sedimentary Systems: From Understanding to Prediction, Special Publication 40, IAS, Wiley-Blackwell 328.

Larue, D.K., Hovadik, J., 2006. Connectivity of channelized reservoirs: A modelling approach. Petroleum Geoscience 12, 291–308.

Parcell, W.C., 2003. Evaluating the development of Upper Jurassic reefs in the Smackover Formation, Eastern Gulf Coast, USA through fuzzy logic computer modeling. Journal of Sedimentary Research 73, 498–515.
Paterson, R.J., Whitaker, F.F., Jones, G.D., Smart, P.L., Waltham, D.A., Felce, G., 2006. Accommodation and sedimentary architecture of isolated icehouse carbonate platforms: Insights from forward modeling with CARB3D. Journal of Sedimentary Research 76, 1162–1182.
Pomar, L., Hallock, P., 2008. Carbonate factories; a conundrum in sedimentary geology. Earth-Science Reviews 87, 134–169.
Press, W.H., Teukolsky, S.A., Vetterling, W.T., Flannery, B.P., 1992. Numerical Recipes in C: The Art of Scientific Computing, second ed. Cambridge University Press, Cambridge 994.
Purkis, S.J., Riegl, B.M., Andrefouet, S., 2005. Remote sensing of geomorphology and facies patterns on a modern carbonate ramp (Arabian Gulf, Dubai, UAE). Journal of Sedimentary Research 75, 861–876.
Schlager, W., 2005. Carbonate Sedimentology and Sequence Stratigraphy: SEPM Concepts in Sedimentology and Paleontology Series No. 8, pp. 200.
Wanless, H.R., Tagett, M.G., 1989. Origin, growth, and evolution of carbonate mudbanks in Florida Bay. Bulletin of Marine Science 44, 454–489.
Wilkinson, B.H., Drummond, C.N., 2004. Facies mosaics across the Persian Gulf and around Antigua—Stochastic and deterministic products of shallow-water sediment accumulation. Journal of Sedimentary Research 74, 513–526.
Williams, H.D., Burgess, P.M., Wright, V.P., Della Porta, G., Granjeon, D., 2011. Investigating carbonate platform types: Multiple controls and a continuum of geometries. Journal of Sedimentary Research 81, 18–37.
Wolfram, S., 2001. A New Kind of Science. Wolfram Media 1197.
Wright, V.P., Burgess, P.M., 2005. The carbonate factory continuum, facies mosaics, and microfacies; an appraisal of some of the key concepts underpinning carbonate sedimentology. Facies 51, 19–25.